Intersubband absorption in $Si_{1-x}Ge_x/Si$ superlattices for long wavelength infrared detectors

Y. Rajakarunanayake and T. C. McGill
California Institute of Technology, Pasadena, California 91125

(Received 31 January 1990; accepted 19 March 1990)

We have calculated the absorption strengths for intersubband transitions in *n*-type $Si_{1-x}Ge_x/Si$ superlattices. These transitions can be used for the detection of long-wavelength infrared radiation. A significant advantage in $Si_{1-x}Ge_x/Si$ superlattice detectors is the ability to detect normally incident light; in $Ga_{1-x}Al_xAs/GaAs$ superlattices intersubband absorption is possible only if the incident light contains a polarization component in the growth direction of the superlattice. We present detailed calculations of absorption coefficients, and peak absorption wavelengths for [100], [111], and [110] $Si_{1-x}Ge_x/Si$ superlattices. Peak absorption strengths of about 2000–6000 cm^{-1} were obtained for typical sheet doping concentrations ($\approx 10^{12}$ cm^{-2}). Absorption comparable to that in $Ga_{1-x}Al_xAs/GaAs$ superlattice detectors, compatibility with existing Si technology, and the ability to detect normally incident light make these devices promising for future applications.

I. INTRODUCTION

Infrared detectors based on intersubband transitions in *n*-type $Ga_{1-x}Al_xAs/GaAs$ superlattices have been investigated extensively in the past few years.[1-8] The detection scheme is based on the excitation of an electron from the conduction band ground state to a higher subband, where it can be swept away by an applied electric field. These detectors have demonstrated promising quantum efficiencies,[7] and are suitable for large area detector array applications in the 8–14 μm range,[3] since planar growth processes such as $Ga_{1-x}Al_xAs/GaAs$ molecular-beam epitaxy (MBE) can insure good uniformity over a large area.[9] Because detection is based on intersubband transitions, these structures are efficient at absorbing radiation in a narrow energy band centered around the subband separation energy. Thus, even with moderate doping concentrations ($\sim 10^{12}$ cm^{-2}), large absorption coefficients of 5000–10 000 cm^{-1} can be achieved.[7] Furthermore, the dependence of the subband energies on superlattice layer thicknesses allows customization of the peak detection wavelength. However, a serious shortcoming of $Ga_{1-x}Al_xAs/GaAs$ superlattice infrared detectors is that the matrix element for absorption of waves incident normal to the interface (polarization parallel to the plane of the quantum wells) is zero.[1] The usefulness of these detectors would be greatly enhanced by the ability to detect normally incident light. Current research on $Ga_{1-x}Al_xAs/GaAs$ superlattice detectors has involved various schemes such as the use of gratings to increase the coupling efficiency of normal illumination.[10] To overcome this difficulty, the $Si_{1-x}Ge_x/Si$ system was proposed by Yang *et al.*[11,12] for making infrared detectors based on intersubband transitions.[12] In general, superlattices composed of indirect materials, where the lowest conduction-band minima are not oriented along the growth direction, show promise of having large optical matrix elements for intersubband transitions for normal incidence.[12,13] To utilize these effects in the $Si_{1-x}Ge_x/Si$ system, however, one must investigate growth in the [111], and [110] directions. In recent years, advances in strained layer $Si_{1-x}Ge_x/Si$ heteroepitaxy by MBE have shown that high quality $Si_{1-x}Ge_x/Si$ superlattices can be grown with good uniformity.[14] In principle, it should be straightforward to extend the $Ga_{1-x}Al_xAs/GaAs$ superlattice infrared detector concept to apply to the $Si_{1-x}Ge_x/Si$ system.

In this paper, we have calculated the absorption coefficients for intersubband transitions in $Si_{1-x}Ge_x/Si$ superlattices grown in the [100], [111], and [110] directions to quantitatively evaluate the merits of this system for detection of infrared radiation. This is the first calculation of the intersubband absorption in $Si_{1-x}Ge_x/Si$ superlattices that has adequately accounted for strain effects,[15,16] and used realistic conduction band offsets.[17] Previous work in this area has assumed infinite barriers, neglected strain effects, and used simplified envelope functions for the calculation of the optical matrix elements.[11-13] We find that finite barrier heights can significantly modify the character of the absorption compared to the infinite barrier case. The motivation for studying [100] oriented $Si_{1-x}Ge_x/Si$ superlattices was to compare absorption strengths with those of $Ga_{1-x}Al_xAs/GaAs$ detectors. Superlattices grown on [111] and [110] orientations were studied because they offer the possibility of obtaining large optical absorption strengths for normal, as well as parallel incidence, making their intersubband absorption properties superior to those of $Ga_{1-x}Al_xAs/GaAs$ superlattices.

In Sec. II of this paper we discuss the theoretical calculations of the superlattice band structure, and of optical absorption coefficients. We analyze the specific dependence of the optical absorption on the reciprocal effective mass tensor, and on the polarization of the incident radiation. In Sec. III, we analyze the conduction-band alignment of $Si_{1-x}Ge_x/Si$ superlattices as a function of strain. We have used the extra degree of freedom offered by strain effects to vary the strain dependent conduction-band positions, thereby obtaining attractive band lineups for superlattice infrared detectors. Based on our analysis of the conduction-band positions, we picked four representative cases for detailed

 0734-211X/90/040929-07$01.00

study. The first case was a [100] $Si_{1-x}Ge_x/Si$ superlattice where the twofold longitudinal minima are the ground state. The second case was a [100] $Si_{1-x}Ge_x/Si$ superlattice where the fourfold transverse minima are the ground state. Results obtained for these two cases determine that [100] $Si_{1-x}Ge_x/Si$ superlattices are just as effective as $Ga_{1-x}Al_xAs/GaAs$ superlattices for detection of infrared radiation at parallel incidence. The third and fourth cases studied were, $Si_{1-x}Ge_x/Si$ superlattices grown in the [111] and [110] directions, respectively. These are the more interesting cases, with nonzero absorption strengths for normal incidence. In Sec. IV, we present absorption coefficients and peak absorption wavelengths for these four cases as functions of the superlattice well and barrier thicknesses. Section V concludes the paper.

II. THEORY

In this section we analyze the optical absorption in an n-type $Si_{1-x}Ge_x/Si$ superlattice due to electron transitions between the first and the second conduction subbands. The absorption coefficient is given by[18]

$$\alpha(\omega)=\frac{4\pi^2e^2}{n_0m^2c\omega}\sum_{n'k',nk}|\langle\psi_{n'k'}|\hat{e}\cdot\mathbf{p}|\psi_{nk}\rangle|^2\times\delta(E_1-E_2+\hbar\omega). \tag{1}$$

Here, m is the free electron mass, e is the electron charge, ω is the angular frequency of the incident light, n_0 is the refractive index at the wavelength of incident light, and ψ_{nk} and $\psi_{n'k'}$ are the initial-state and final-state electron wave functions, respectively. We have denoted the bulk band indices by the labels n and n', and the electron wave vectors by k and k'. Thus, intersubband transitions are when $n=n'$. This expression must be summed over all the bands that contribute to the transition. The vector $\hat{e}$ denotes the polarization direction of the incident radiation, and $\mathbf{p}$ denotes the momentum operator. If the above matrix element is evaluated by writing each of the wave functions as a product of a periodic Bloch function and a slowly varying envelope function, one then, by taking into account the change in the Bloch function away from the center of the critical point (the Δ minimum in this case) and restricting the analysis to intersubband transitions, recovers a simple expression for the matrix element based on the effective mass. The derivation of this result is quite similar to the proof of the effective mass theorem given by Kohn and Luttinger.[19]

For the rest of this paper, we assume without loss of generality that the growth axis is always denoted by the z axis. We can then write the matrix element for intersubband transitions

$$\langle\psi_{nk}|\hat{e}\cdot\mathbf{p}|\psi_{nk}\rangle=\langle F_{k'}(z)|\hat{e}_i\left(\frac{1}{m^*_{iz}}\right)p_z|F_k(z)\rangle. \tag{2}$$

In Eq. (2), $1/m^*_{ij}$ are the components of the dimensionless reciprocal effective mass tensor. Summation over repeated indices is assumed in the usual fashion. $F_k(z)$ and $F_{k'}(z)$ denote the envelope functions of the first and second conduction subbands, respectively. Using Eq. (2), we can rewrite Eq. (1) as

$$\alpha(\omega)=\frac{4\pi^2e^2\hbar^2}{n_0m^2c\omega}\int|\langle F_{k'}(z)\nabla_zF_k(z)\rangle|^2\times\left(\frac{\hat{e}_x}{m^*_{xz}}+\frac{\hat{e}_y}{m^*_{yz}}+\frac{\hat{e}_z}{m^*_{zz}}\right)^2\times\frac{d^3k}{4\pi^2}\delta(E_1-E_2+\hbar\omega). \tag{3}$$

From the above equation, it is easy to see that nonzero absorption strengths for normal incidence ($\hat{e}_x,\hat{e}_y\neq0$; $\hat{e}_z=0$) can be achieved only when $1/m^*_{xz}$ or $1/m^*_{yz}$ are nonzero. This occurs when the growth direction is misaligned with respect to the principal axes of the ellipsoidal valleys.

If we denote the sheet doping concentration per superlattice layer by N_S, then assuming a zero temperature, two-dimensional Fermi distribution and assuming that the envelope function matrix element is independent of $\mathbf{k}_\parallel$ and $\mathbf{k}_\perp$, we can evaluate the integral over $dk_x\,dk_y$ (parallel to the superlattice planes). We can also write the delta function in the above equation as a normalized Lorentzian with a broadening parameter Γ, to account for the excited state lifetime τ (given by $\Gamma=\hbar/\tau$). The expression for $\alpha(\omega)$ then becomes

$$\alpha(\omega)=\frac{4\pi e^2\hbar^2}{n_0m^2c\omega}|\langle F_2(z)\nabla_zF_1(z)\rangle|^2\times\left(\frac{\hat{e}_x}{m^*_{xz}}+\frac{\hat{e}_y}{m^*_{yz}}+\frac{\hat{e}_z}{m^*_{zz}}\right)^2\times N_S\int_0^{\pi/L}\frac{(\Gamma/2\pi)dk_z}{[\hbar\omega-E_{12}(k_z)]^2+\Gamma^2/4}. \tag{4}$$

Here, L is the length of a period of the superlattice, and $E_{12}(k_z)$ is the subband separation energy. Equation (4) shows that absorption is proportional to the sheet doping concentration N_S. Furthermore, if there is only a very small amount of dispersion in $E_{12}(k_z)$, then $\alpha(\omega)$ is inversely proportional to the bandwidth Γ and superlattice period L. In the actual calculations reported here, we have retained the dependence of the matrix element on $\mathbf{k}_\parallel$ and $\mathbf{k}_\perp$, as in Eq. (3). However, we have assumed a zero temperature Fermi distribution, and a broadening parameter Γ of 8 meV. We have also assumed a sheet doping concentration of 10^{12} cm^{-2}.

In our calculations, we first study the band structure of the $Si_{1-x}Ge_x$ host layers using full zone $\mathbf{k}\cdot\mathbf{p}$ theory.[20-22] We obtain alloy parameters by averaging the input $\mathbf{k}\cdot\mathbf{p}$ parameters for Si and Ge. A more detailed description of the band structure calculations for $Si_{1-x}Ge_x/Si$ superlattices is given elsewhere.[22] We construct the envelope functions for the superlattice states by matching the wave function and probability current density at the interfaces, then impose the Bloch condition on the superlattice unit cells to obtain the subband structure of the superlattice. For ease of calculations, however, we have approximated the multicomponent envelope function of full zone $\mathbf{k}\cdot\mathbf{p}$ theory by a single wave function that corresponds to a given ellipsoidal Δ valley. This approximation also neglects effects due to intervalley interference that would be present if the complete full zone $\mathbf{k}\cdot\mathbf{p}$ wave functions are considered. We have confirmed that this simplified approach gives excellent agreement (energy

positions within 1–2 meV) with the results of a more complicated model[22] in which the band structure of $Si_{1-x}Ge_x$/Si [100] superlattices is calculated with a multi component envelope function.

III. STRAIN EFFECTS

Because of the lattice mismatch between Si and Ge ($\approx$4.2%), strain plays a crucial role in determining the relevant conduction-band offsets. To achieve substantial optical matrix elements, it is important to have a large conduction-band offset between the well and the barrier; this is because, the superlattice approaches a uniform alloy as the barrier height goes to zero, and the intersubband matrix elements therefore also approach zero. In our calculations we have assumed an average valence-band offset of $\Delta E_V^{av} = 0.54 \pm 0.04$ eV, in accordance with the calculations of Van de Walle and Martin.[17,23] This value for the band offset is also in close agreement with the experimental value reported by Yu *et al.*[24] obtained using x-ray photoelectron spectroscopy. We have used the phenomenological deformation potential theory[25,26] to describe the shifts in the conduction-band positions as a function of strain; our calculations of the strain dependence of the band edge positions are in close agreement with those of Van de Walle and Martin.[17,23] A more detailed discussion of strain effects in $Si_{1-x}Ge_x$/Si superlattices is given elsewhere.[27]

The position of the conduction-band edge depends on the distribution of strain in the epilayer. We assume that the entire superlattice structure is coherently strained to the buffer layer; this assumption is valid if the epitaxial layers do not exceed the critical thickness for pseudomorphic growth.[28,29] In order to satisfy this condition, we have limited our structures to contain only layers thinner than 60 monolayers, and the maximum difference in alloy concentration we allow across an interface is 60%, corresponding to a lattice mismatch of less than 2.4%.

Figures 1(a) and 1(b) show the strain split Δ conduction-band minima for $Si_{1-x}Ge_x$ epilayers grown on Si and Ge buffer layers, respectively. The zero of energy is the position of the unstrained valence-band maximum of Si. For growth on [100] buffer layers, the conduction bands are split into twofold longitudinal and fourfold transverse valleys. For [111] growth, the sixfold degeneracy of the Δ conduction-band minima is not broken. For [110] growth, the conduction bands are again split into twofold transverse valleys, and fourfold valleys tilted 45° to the growth axis.

The first case we examine is absorption from twofold longitudinal electrons in [100] $Si_{1-x}Ge_x$/Si superlattices. Figure 1(b), shows that the ground state will be the twofold valleys for superlattices consisting of Si-rich well layers, and Ge-rich barrier layers, coherently strained to a Ge-rich [100] buffer layer. The variation of the twofold band edge position as a function of the alloy composition is quite large for the [100] growth direction, making it easy to achieve large conduction band offsets. The second case of interest is absorption from the fourfold transverse electrons in [100] $Si_{1-x}Ge_x$/Si superlattices. From Fig. 1(a), we see that the fourfold states would be lowest when the superlattice consists of Si-rich well layers and Ge-rich barrier layers, coher-

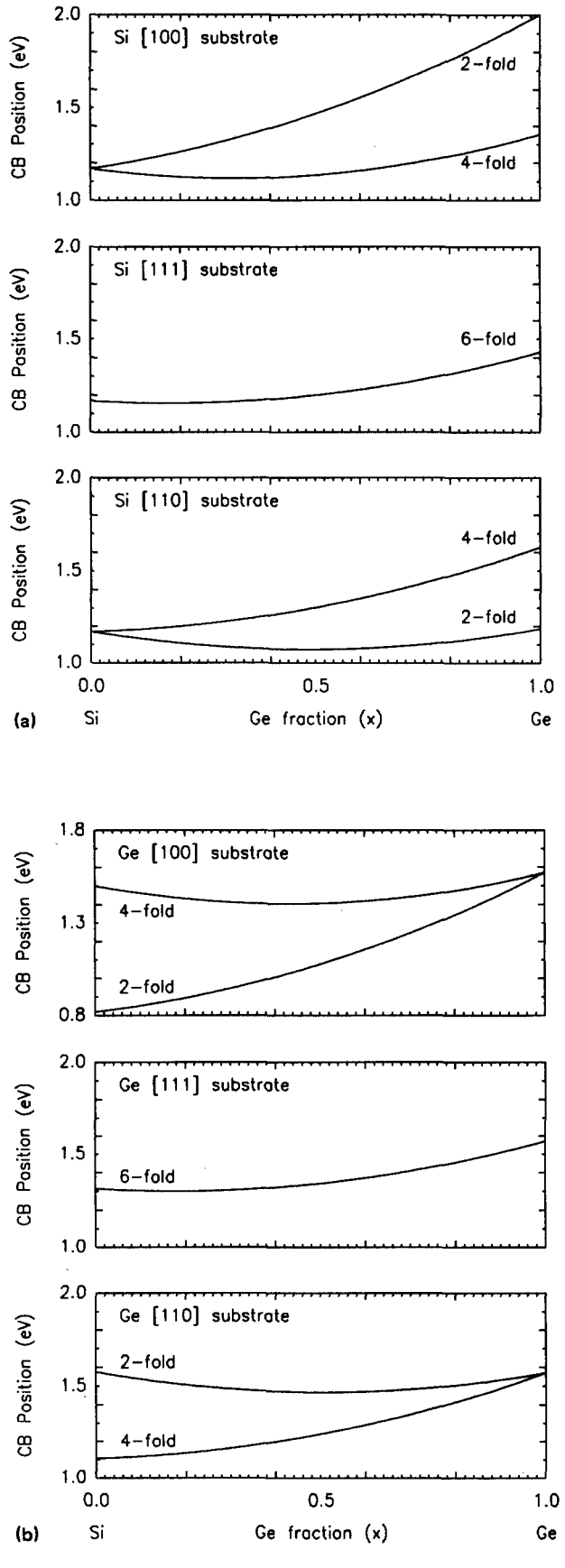

FIG. 1 The variation of the conduction-band positions of the strain split Δ conduction valleys for coherently strained $Si_{1-x}Ge_x$ epilayers is shown for growth on (a) Si, and (b) Ge buffer layers. The results are presented for [100], [111], and [110] growth orientations.

ently strained to a Si-rich [100] buffer layer. However, it is difficult to achieve a significant conduction-band offset for these fourfold states. In order to obtain the maximum barrier heights, the composition of the well layer should be at the minimum of the band bowing region ($\approx$30% Ge concentration) of the fourfold conduction band of Fig. 1(a).

The third case we study is that of [111] $Si_{1-x}Ge_x$/Si superlattices. The sixfold degeneracy of the Δ conduction-band minima is not broken for growth in the [111] direction. In order to achieve the maximum barrier heights, we pick a well layer close to the minimum of the slight band bowing region ($\approx$20% Ge concentration), and a Ge-rich barrier layer ($\approx$80% Ge concentration). The choice of the buffer layer is not critical since strain effects shift all the valley positions equally. The fourth we consider is that of [110] oriented $Si_{1-x}Ge_x$/Si superlattices. For [110] growth, strain effects split the conduction bands into twofold and fourfold components. In this case, however, the fourfold states are ellipsoids oriented at 45° to the growth axis, and the twofold states are transverse ellipsoids. The fourfold states are the more interesting ones, showing the possibility of absorption at normal incidence. A fourfold ground state can be achieved in a structure in which Si-rich well layers and Ge-rich barrier layers are grown coherently strained to a Ge-rich buffer layer.

IV. RESULTS

In Figs. 2(a) and 2(b), we show the intersubband absorption coefficient for [100] $Si_{1-x}Ge_x$/Si superlattices calculated using Eq. (3). The structure we consider is a superlattice with Si well layers and $Si_{0.4}Ge_{0.6}$ barrier layers coherently strained to a $Si_{0.4}Ge_{0.6}$ buffer layer. This band alignment has the twofold longitudinal electrons in the ground state. The results are presented for the absorption of light at parallel incidence to the superlattice, since normally incident light cannot be absorbed in this configuration. The $Si_{0.4}Ge_{0.6}$ buffer layer was chosen to push the fourfold valleys higher in energy compared to the twofold valleys. This choice for the buffer layer limits the maximum overall thickness for a coherently strained superlattice, since a $Si_{0.4}Ge_{0.6}$/Si superlattice in its free-standing configuration will have a different in-plane lattice constant than a $Si_{0.4}Ge_{0.6}$ buffer layer. If we pick a buffer layer that was lattice matched to the free-standing lattice constant of the superlattice, then much thicker superlattices can be considered. However, the separation between the twofold and fourfold levels would then be smaller, and the fourfold states may interfere with the absorption of the twofold states. Figure 2(a) shows that fairly good absorption can be achieved for barrier and well widths of about 20 monolayers. The apparent decrease in absorption at large layer thicknesses is an artifact of the way we present the results. Because we have assumed a constant doping concentration per superlattice unit cell (constant sheet doping concentration), as the unit cell size of the superlattice increases, the effective bulk doping concentration decreases, reducing the absorption. In Fig. 2(b) we show the peak absorption wavelength in μm for transitions from the first to the second conduction subbands. The wavelength range of interest for atmospheric communications (8–14 μm) occurs for Si well thicknesses of 12–20 monolayers. As seen in Fig. 2(b), the quantum well level separations are mainly determined by the well thicknesses and not by the barrier thicknesses, since the barrier heights are fairly large and the masses of the longitudinal electrons are large ($\approx$0.98 m).

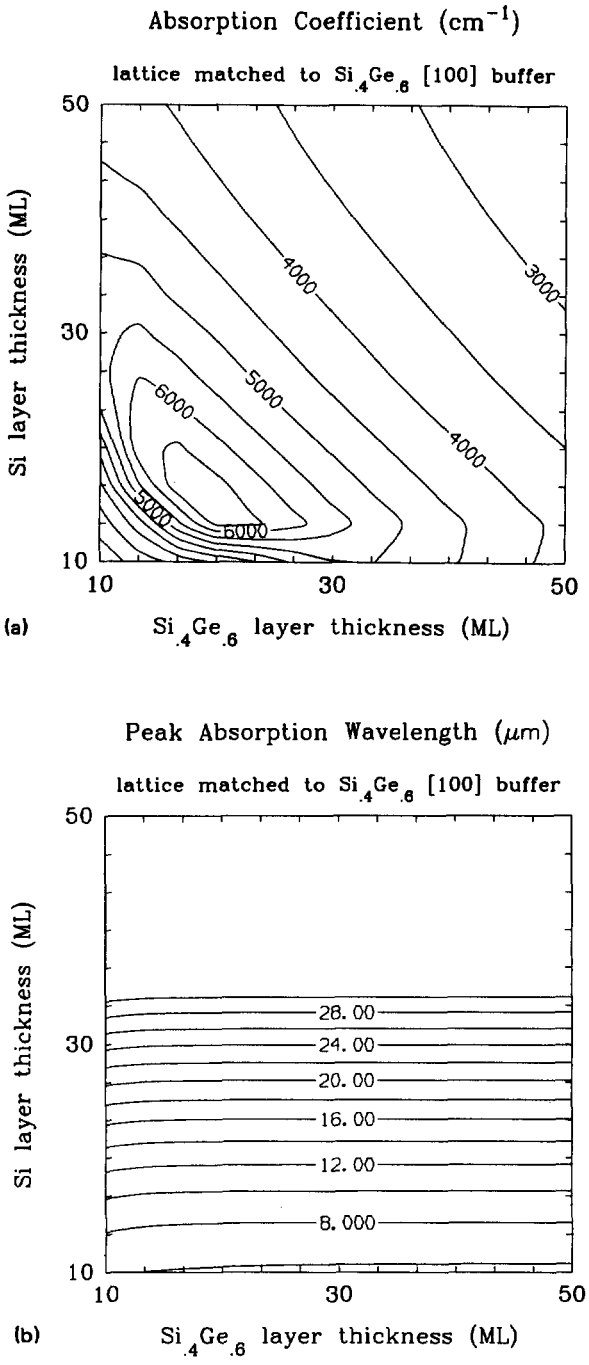

FIG. 2. (a) Absorption coefficients, and (b) peak absorption wavelengths for light at parallel incidence for a [100] Si/$Si_{0.4}Ge_{0.6}$ superlattice. In this case, the twofold longitudinal conduction valleys are in the ground state. The superlattice is assumed to be coherently strained to a $Si_{0.4}Ge_{0.6}$ buffer layer. The contour lines show the variation of the absorption coefficient, and peak absorption wavelength as a function of the Si well thickness and $Si_{0.4}Ge_{0.6}$ barrier thickness. The layer thicknesses are measured in monolayers, denoted by ML in the figures.

In Figs. 3(a) and 3(b), we show the intersubband absorption coefficients, and peak absorption wavelengths, respectively, for [100] $Si_{1-x}Ge_x$/Si superlattices, when the fourfold transverse valley electrons are in the ground state. Results are again presented for parallel incidence, since absorption at normal incidence does not occur. We have considered a $Si_{0.7}Ge_{0.3}$ well layer and a $Si_{0.2}Ge_{0.8}$ barrier layer coherently strained to a $Si_{0.7}Ge_{0.3}$ buffer layer. A higher concentration of Ge in the barrier layer would not be desirable, since above $\approx 85\%$ Ge concentration the conduction-band minimum of $Si_{1-x}Ge_x$ alloys changes from a Si-like Δ minimum to a Ge-like L minimum.[17] The $Si_{0.7}Ge_{0.3}$ buffer layer was chosen to push the twofold valleys as high in energy as possible compared to the fourfold valleys. Although a buffer layer lattice matched to the free-standing $Si_{0.7}Ge_{0.3}/Si_{0.2}Ge_{0.8}$ superlattice would be more appropriate for thick superlattices, the smaller twofold/fourfold splitting might significantly influence the absorption from the fourfold valleys. The peak absorption coefficients for fourfold electrons occur at wavelengths of 20–30 μm for the layer thickness range shown in Fig. 3(a). This makes the absorption from fourfold electrons less attractive than the absorption from the twofold electrons for detection in the atmospheric window. The qualitative features of the contour lines in Fig. 3(a) are quite different from Fig. 2(a) because the small barrier heights, and the small effective masses influence the absorption coefficients significantly. The optical matrix elements are still increasing as a function of the well layer thickness at 60 monolayers for fourfold electrons, and the decrease in absorption occurs at much larger layer thicknesses than for the twofold case. The smaller effective masses of the fourfold states (≈ 0.19 m) result in slightly larger absorption coefficients for fourfold electrons than for twofold electrons.

Our analysis of the absorption properties of the twofold and fourfold electrons for [100] oriented $Si_{1-x}Ge_x$/Si superlattices shows that twofold electrons are more suitable for applications in the 8–14 μm range. The potential increase in the absorption that could have been achieved with fourfold electrons because of smaller effective masses is outweighed by the decrease in the optical matrix elements due to smaller conduction-band offsets and poor confinement of the envelope functions. We also find that because of poor carrier confinement, it is quite difficult to push the peak absorption wavelength of the fourfold valleys to the 8–14 μm range.

Results for [111] $Si_{1-x}Ge_x$/Si superlattices are shown in Figs. 4(a) and 4(b). In Fig. 4(a), we show the absorption coefficient for normally incident light. These results are for a [111] $Si_{1-x}Ge_x$/Si superlattice with $Si_{0.8}Ge_{0.2}$ well layers and $Si_{0.2}Ge_{0.8}$ barrier layers grown coherently strained to a [111] $Si_{0.5}Ge_{0.5}$ buffer layer. There is no preferred azimuthal polarization direction for absorption of normally incident light in this case. This growth direction preserves the sixfold degeneracy of the Δ conduction valleys, and electrons from all six valleys contribute to the absorption. The choice of the buffer layer is not critical in this case, and we have therefore considered a $Si_{0.5}Ge_{0.5}$ buffer layer, quite closely lattice matched to the free-standing $Si_{0.2}Ge_{0.8}/Si_{0.8}Ge_{0.2}$ superlattice. The obvious advantage of considering such a buffer layer is the ability to grow thicker coherently strained structures.[30] The contour plot of the absorption shown in Fig. 4(a) is qualitatively similar to an intermediate case between Figs. 2(a) and 3(a); the peak in Fig. 4(a) occurs at a larger layer thickness than in Fig. 2(a), but at a

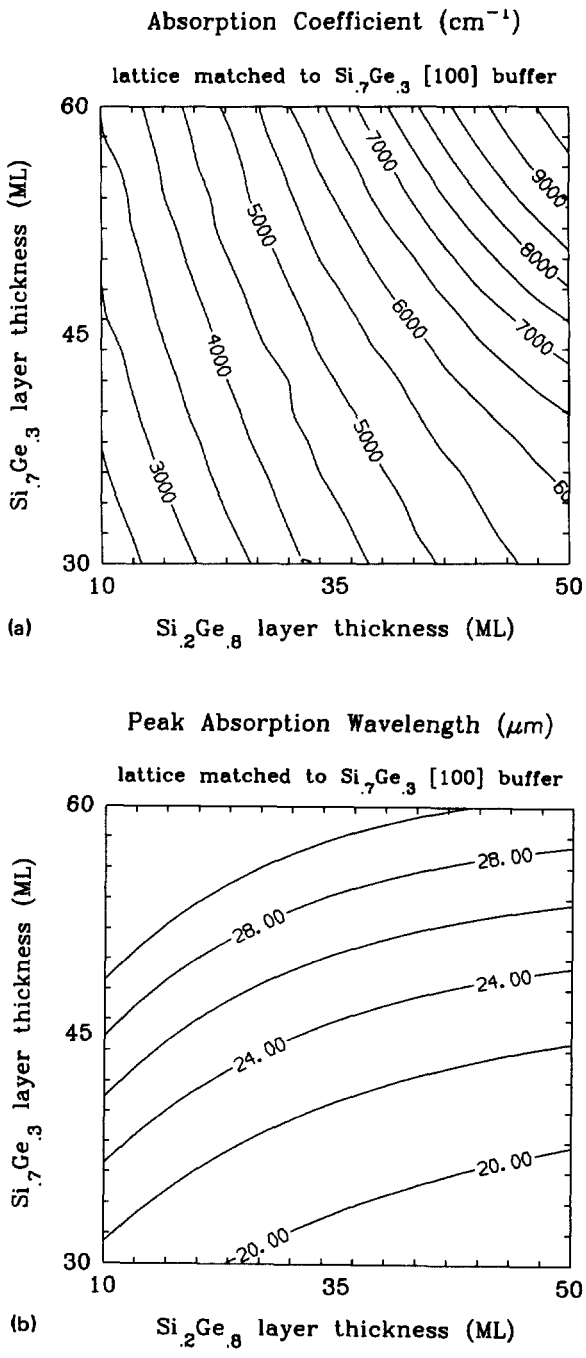

FIG. 3. (a) Absorption coefficients, and (b) peak absorption wavelengths for light at parallel incidence for a [100] $Si_{0.7}Ge_{0.3}/Si_{0.2}Ge_{0.8}$ superlattice. In this case, the fourfold transverse conduction valleys are in the ground state. The superlattice is assumed to be coherently strained to a $Si_{0.7}Ge_{0.3}$ buffer layer. The contour lines show the variation of the absorption coefficient, and peak absorption wavelength as a function of the $Si_{0.7}Ge_{0.3}$ well thickness and $Si_{0.2}Ge_{0.8}$ barrier thickness. The layer thicknesses are measured in monolayers, denoted by ML in the figures.

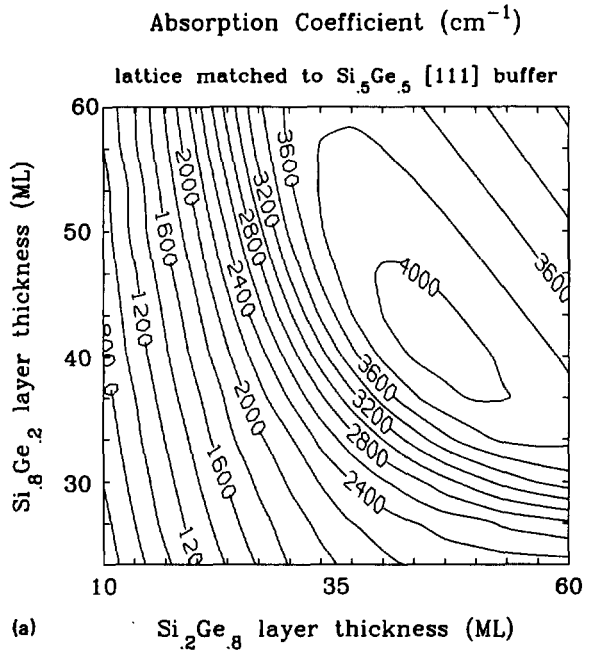

FIG. 4. (a) Absorption coefficients, and (b) peak absorption wavelengths for light at normal incidence for a [111] $Si_{0.8}Ge_{0.2}/Si_{0.2}Ge_{0.8}$ superlattice. In this case, the sixfold degenerate Δ conduction valleys are in the ground state. The superlattice is assumed to be coherently strained to a $Si_{0.5}Ge_{0.5}$ buffer layer. The contour lines show the variation of the absorption coefficient, and peak absorption wavelength as a function of the $Si_{0.8}Ge_{0.2}$ well thickness and $Si_{0.2}Ge_{0.8}$ barrier thickness. The layer thicknesses are measured in monolayers, denoted by ML in the figures.

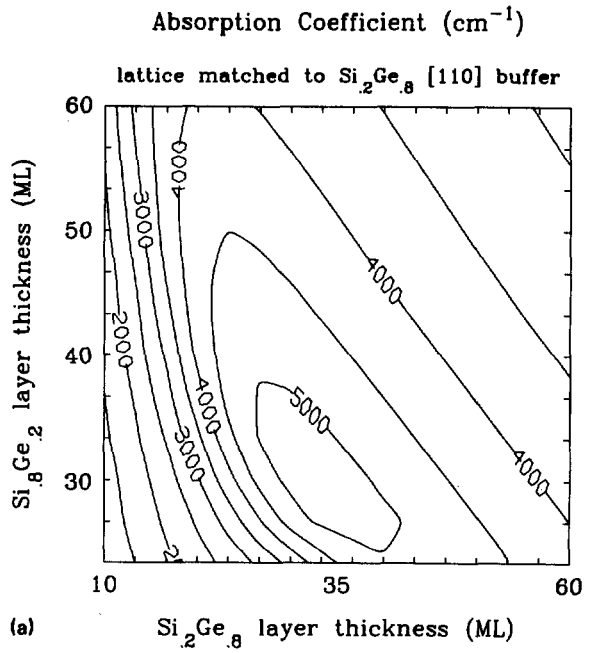

FIG. 5. (a) Absorption coefficients, and (b) peak absorption wavelengths for light at normal incidence for a [110] $Si_{0.8}Ge_{0.2}/Si_{0.2}Ge_{0.8}$ superlattice. In this case, the fourfold valleys that are oriented at 45° to the growth axis are in the ground state. The superlattice is assumed to be coherently strained to a $Si_{0.2}Ge_{0.8}$ buffer layer. The contour lines show the variation of the absorption coefficient, and peak absorption wavelength as a function of the $Si_{0.8}Ge_{0.2}$ well thickness and $Si_{0.2}Ge_{0.8}$ barrier thickness. The layer thicknesses are measured in monolayers, denoted by ML in the figures.

smaller layer thickness than where the peak in Fig. 3(a) would be (not shown in figure). This is because the barrier heights and the effective masses in the growth direction for Fig. 4(a), lie in between the values for Figs. 2(a) and 3(a). The peak absorption wavelengths of Fig. 4(b) occur closer to the 8–14 μm range than in Fig. 3(b), making the [111] $Si_{1-x}Ge_x$/Si superlattices more useful than [100] $Si_{1-x}Ge_x$/Si superlattice with fourfold electrons for infrared applications. Figure 4(a) shows that a peak absorption coefficient of 4000 cm^{-1} can easily be achieved for moderate sheet doping concentrations of 10^{12} cm^{-2}.

Calculations for [110] $Si_{1-x}Ge_x$/Si superlattices are

shown in Figs. 5(a) and 5(b). In Fig. 5(a), we show the absorption coefficient for normally incident light. These results correspond to a [110] $Si_{1-x}Ge_x$/Si superlattice with $Si_{0.8}Ge_{0.2}$ well layers and $Si_{0.2}Ge_{0.8}$ barrier layers grown coherently strained to a [111] $Si_{0.2}Ge_{0.8}$ buffer layer. In these superlattices, the ground state consists of the fourfold conduction valleys that are oriented at 45° to the growth axis. There is a preferred azimuthal direction to the absorption, with peak absorption occurring for light polarized along the $[1\bar{1}0]$ azimuthal direction, zero absorption occurring for light polarized along the [001] azimuthal direction. The matrix elements are slightly larger than for the [111] $Si_{1-x}Ge_x$/Si superlattices due to the larger [110] fourfold conduction-band offsets which give rise to larger intersubband matrix elements. The $Si_{0.2}Ge_{0.8}$ buffer layer was chosen to push the twofold valleys higher in energy compared to the fourfold valleys. For this choice of the buffer layer, the maximum overall thickness for a coherently strained superlattice will be limited by the critical thickness for strain relaxation.[28–30] If, on the other hand, if we pick a buffer layer that was lattice matched to the free-standing lattice constant of the superlattice, then much thicker superlattice layers can be considered. However, the separation between the fourfold and twofold levels would be smaller; the twofold states could then interfere with the absorption of the fourfold states and reduce the efficiency of detection at normal incidence. Figure 5(a) shows that an absorption coefficient of 5000 cm^{-1} can easily be achieved for moderate sheet doping concentrations of 10^{12} cm^{-2}. The absorption shown in Fig. 5(a) is qualitatively similar to Fig. 2(a). The peak wavelength of absorption also occurs in the 8–14 μm region making these superlattices good candidates for detection in the atmospheric window.

V. CONCLUSIONS

We have calculated intersubband absorption strengths for [100], [111], and [110] oriented $Si_{1-x}Ge_x$/Si superlattices. We have shown that the absorption strengths obtained in all three of these directions are comparable to those found in [100] $Ga_{1-x}Al_xAs$/GaAs superlattices. Absorption in [111] and [110] $Si_{1-x}Ge_x$/Si superlattices is superior to that in [100] $Ga_{1-x}Al_xAs$/GaAs superlattices because normally incident light can be absorbed. We find that it is possible to achieve absorption coefficients of about 5000 cm^{-1} for normally incident radiation in the 8–14 μm region by using [110] oriented $Si_{1-x}Ge_x$/Si superlattices with sheet doping concentrations of 10^{12} cm^{-2}. Our results indicate that these superlattices should be extremely promising candidates for long wavelength infrared detectors.

ACKNOWLEDGMENTS

This work was supported by the Defense Advanced Research Projects Agency, under Contract No. N00014-89-J-3196. We also like to acknowledge useful discussions with R. J. Hauenstein, E. T. Yu, R. H. Miles, and D. L. Smith.

[1] L. C. West and S. J. Eglash, Appl. Phys. Lett. **46**, 1156 (1985).
[2] D. D. Coon and R. P. G. Karunasiri, Appl. Phys. Lett. **45**, 649 (1984).
[3] E. L. Dereniak and D. G. Crowe, *Optical Radiation Detectors* (Wiley, New York, 1984).
[4] B. F. Levine, K. K. Choi, C. G. Bethea, J. Walker, and R. J. Malik, Appl. Phys. Lett. **51**, 934 (1987).
[5] B. F. Levine, K. K. Choi, C. G. Bethea, J. Walker, and R. J. Malik, Appl. Phys. Lett. **50**, 1092 (1987).
[6] K. K. Choi, B. F. Levine, C. G. Bethea, J. Walker, and R. J. Malik, Appl. Phys. Lett. **50**, 1814 (1987).
[7] B. F. Levine, C. G. Bethea, G. Hasnain, J. Walker, and R. J. Malik, Appl. Phys. Lett. **53**, 296 (1988).
[8] L. Esaki and H. Sakaki, IBM Tech. Discl. Bull. **20**, 2456 (1977).
[9] *Gallium Arsenide Technology*, edited by D. K. Ferrey (Sams, Indianapolis, 1985).
[10] K. W. Goossen, S. A. Lyon, and K. Alavi, Appl. Phys. Lett. **53**, 1027 (1988).
[11] C. I. Yang and D. S. Pan, J. Appl. Phys. **64**, 1573 (1988).
[12] C. I. Yang, D. S. Pan, and R. Somoano, J. Appl. Phys. **65**, 3253 (1989).
[13] E. R. Brown and S. J. Eglash, Phys. Rev. B (to be published).
[14] E. Kasper and J. C. Bean, *Silicon Molecular Beam Epitaxy* (Chemical Rubber, Boca Raton, FL, 1987).
[15] R. People, Phys. Rev. B **32**, 1405 (1985).
[16] R. People and J. C. Bean, Appl. Phys. Lett. **48**, 538 (1986).
[17] C. G. Van de Walle and R. M. Martin, Phys Rev. B **34**, 5621 (1986).
[18] F. Bassani, *Electronic States and Optical Transitions in Solids* (Pergamon, New York, 1973).
[19] J. M. Luttinger and W. Kohn, Phys. Rev. **97**, 869 (1955).
[20] M. Cardona and F. H. Pollack, Phys. Rev. **142**, 530 (1966).
[21] C. W. Higginbotham, Ph.D. thesis, Brown University, 1970.
[22] Y. Rajakarunanayake and T. C. McGill, Phys. Rev. B **40**, 3051 (1989).
[23] C. G. Van de Walle and R. M. Martin, J. Vac. Sci. Technol. B **3**, 1256 (1985).
[24] E. T. Yu, E. T. Croke, T. C. McGill, and R. H. Miles, Appl. Phys. Lett. **56**, 569 (1990).
[25] H. Hesagawa, Phys. Rev. **129**, 1029 (1963).
[26] J. C. Hensel and G. Feher, Phys. Rev. **129**, 1041, (1963).
[27] Y. Rajakarunanayake and T. C. McGill, J. Vac. Sci. Technol. B **4**, 799 (1989).
[28] R. People and J. C. Bean, Appl. Phys. Lett. **47**, 322 (1985).
[29] J. C. Matthews and A. E. Blakeslee, J. Cryst. Growth **27**, 118 (1974).
[30] R. H. Miles, T. C. McGill, S. Sivananthan, X. Chu, and J. P. Faurie, J. Vac. Sci. Technol. B **5**, 1263 (1987).